

# ARS-DETR: Aspect Ratio Sensitive Oriented Object Detection with Transformer

Ying Zeng<sup>1</sup>, Xue Yang<sup>2\*</sup>, Qingyun Li<sup>1</sup>, Yushi Chen<sup>1\*</sup>, Junchi Yan<sup>2</sup>

<sup>1</sup>Harbin Institute of Technology <sup>2</sup>Shanghai Jiao Tong University

{22S005064, 21B905003, chen yushi}@stu.hit.edu.cn {yangxue-2019-sjtu, yanjunchi}@sjtu.edu.cn

<https://github.com/httle/ARS-DETR>

## Abstract

Existing oriented object detection methods commonly use metric  $AP_{50}$  to measure the performance of the model. We argue that  $AP_{50}$  is inherently unsuitable for oriented object detection due to its large tolerance in angle deviation. Therefore, we advocate using high-precision metric, e.g.  $AP_{75}$ , to measure the performance of models. In this paper, we propose an Aspect Ratio Sensitive Oriented Object Detector with Transformer, termed ARS-DETR, which exhibits a competitive performance in high-precision oriented object detection. Specifically, a new angle classification method, calling Aspect Ratio aware Circle Smooth Label (AR-CSL), is proposed to smooth the angle label in a more reasonable way and discard the hyperparameter that introduced by previous work (e.g. CSL). Then, a rotated deformable attention module is designed to rotate the sampling points with the corresponding angles and eliminate the misalignment between region features and sampling points. Moreover, a dynamic weight coefficient according to the aspect ratio is adopted to calculate the angle loss. Comprehensive experiments on several challenging datasets show that our method achieves competitive performance on the high-precision oriented object detection task.

## 1. Introduction

Oriented object detection is a recently emerged task in computer vision [4, 41, 33, 6]. Compared with the generic detection, oriented object detection could provide more accurate orientation and scale information to localize object and exhibits a stronger ability to process and understand visual information in aerial images [39], scene text [49], face[24] and 3-D objects [48] etc.

$AP_{50}$  is the most common metric used in oriented object detection and many works compare the performance according to  $AP_{50}$ . However, we want to raise a question here: **Could  $AP_{50}$  well reflect the performance of ori-**

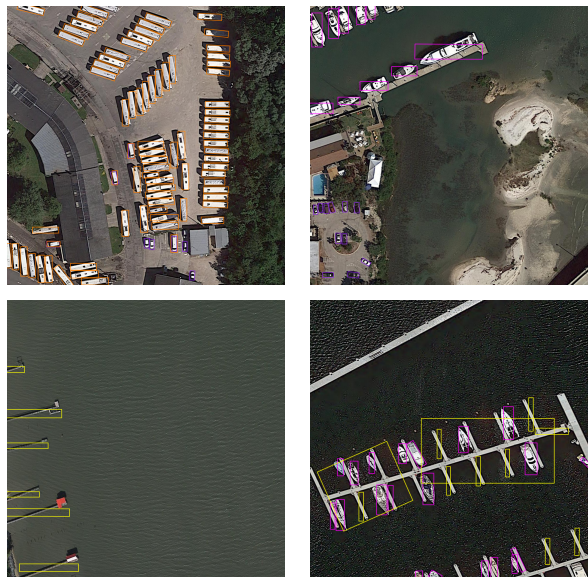


Figure 1. Even though the angle prediction is inaccurate, it still obtains a high performance in terms of  $AP_{50}$ . This phenomenon shows that  $AP_{50}$  is inherently unsuitable for oriented object detection due to its large tolerance in angle deviation.

**ented object detectors?** Maybe not, according to our findings. Fig. 1 shows the visualization of some detectors. It can be found that the centering points, length and width of some bounding boxes are very close to the objects, but the angle deviates a lot. Even so, most of them will still be detected as positive and will achieve a high performance in terms of  $AP_{50}$ . Therefore, this abnormal phenomenon urges us to advocate the use of more stringent metric (e.g.  $AP_{75}$ ) to evaluate the performance, and to focus on more meaningful high-precision oriented object detection.

Angle, as a unique parameter in oriented object detection, plays a vital role in high-precision detection. Among a large number of angle prediction methods, classification-based method shows a favorable performance [36, 34, 28]. Specifically, it decouples the angle from the bounding boxes and transform the angle prediction into a classification task, which eliminates the boundary issue [40]. Moreover, TIOE

\*Corresponding authors.

[21] also shows a strong potential of classification-based method in high-precision oriented object detection. Nevertheless, there still exist some issues, such as ignoring the correlation between the angle and bounding boxes completely, introducing hyperparameter (e.g. window radius in CSL [36]), and etc. Hence, the accuracy of the angle prediction is hindered to some extent.

Recently, the Transformer based detectors [1, 51] have revived object detection task again. Without additional complicated hand-designed components like preset Anchor or Non-Maximum Suppression (NMS), DETR with Transformer (DETR [1]) regards object detection as a set prediction task and assigns labels by bipartite graph matching, which achieves a comparable performance with classical detectors like Faster RCNN [23]. Existing DETR derivatives [51, 20, 11, 46, 29, 15] dramatically improve detection performance and convergence speed, exhibiting great potential of Transformer for high-precision object detection. Although some DETR-based oriented object detection methods [19, 3] have been proposed, they still use regression to predict angle and do not take into account the issues caused by boundary discontinuity. Meanwhile, they predict angle in a naive way and do not explore how to embed angle information into DETR. How to use DETR more naturally in oriented object detection is still a research topic.

In this paper, we propose an Aspect Ratio Sensitive Deformable DETR-based oriented object detection, called ARS-DETR. Specifically, an hyperparametric free Aspect Ratio aware Circle Smooth Label (AR-CSL) is designed to represent the relationship of adjacent angles according to the aspect ratio of the object. Considering the sensitivity of different objects to angle, AR-CSL uses the SkewIoU of the objects with different aspect ratios under each angle deviation to smooth the angle label. Then, We also propose a rotated deformable attention module to embed the angle information into the DETR-based detector to align the feature. Finally, we adopt the aspect ratio aware loss and matching strategy to make the training of the detector can be adjusted dynamically, which can greatly reduce the burden of model training. Extensive experiments show that ARS-DETR is indeed an excellent detector in high-precision oriented object detection on different datasets. In summary, our contributions lie in four-folds as follows:

- We summarize the influence of angle deviation in the oriented object detection and the flaws of the current oriented object detection metric (e.g.  $AP_{50}$ ) in detail, and advocate to use more stringent metric (e.g.  $AP_{75}$ ) to evaluate the performance of the model, inspiring researchers to pay more attention to the high-precision oriented object detection.
- A new angle classification method called Aspect Ratio aware Circle Smooth Label (AR-CSL), which adopts

the value of the SkewIoU of objects with different aspect ratio under each angle deviation, is designed to smooth angle labels in a more reasonable way while eliminating the hyperparameter of window radius introduced by previous work.

- We propose an angle embedded rotated deformable attention module to align the feature, and combined with the new angle classification technique (i.e. AR-CSL), denoising strategy (DN), and aspect ratio sensitive weighting (ARW) and matching (ARM) to further improve the performance.
- Extensive experiments on three public datasets: DOTA-v1.0, DIOR-R and OHD-SJTU demonstrate the effectiveness of the proposed model. ARS-DETR achieves the state-of-the-art performance on the  $AP_{75}$  in the all datasets.

## 2. Related Work

### 2.1. Angle Classification based Oriented Detection

As an emerging task, oriented object detection has made great progress in recent years. The mainstream regression angle prediction methods [18, 41, 4] often suffer from boundary discontinuity [36], so the classification based angle prediction methods are proposed. CSL [36] transforms the prediction from of angle from regression to classification to eliminate the boundary issue by designing a Circle Smooth Label. DCL [34, 37] uses dense coded label to reduce the amount of computation and parameters of CSL. GF-CSL [28] adopts a dynamic weighting mechanism based on CSL to perform precise angle estimation for rotated objects. To overcome the challenges of ambiguity and high costs in angle representation, MGAR [27] proposes a multi-grained angle representation method, consisting of coarse-grained angle classification and fine-grained angle regression. TIOE [21] proposes a progressive orientation estimation strategy to approximate the orientation of objects with n-ary codes. PSC [45] provides a unified framework for various periodic fuzzy issues in oriented object detection by mapping rotational periodicity of different cycles into phase of different frequencies. AR-BCL [31] uses an aspect ratio-based bidirectional coded label to solve the square-like detection issue [34]. In contrast, the new angle encoding technique proposed in this paper is free from hyperparameters, boundary issue, and square-like issue, and further explores the potential of angle classification in high-precision detection, which is not considered by most of the above methods.

### 2.2. DETR and Its Variants

DETR [1] proposed a Transformer-based end-to-end object detector without using hand-designed components like

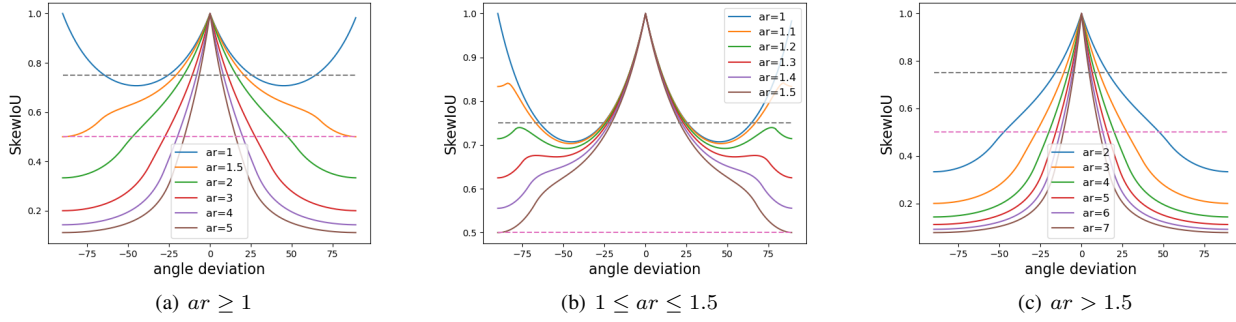


Figure 2. The curve between SkewIoU and angle deviation under different aspect ratio.  $ar$  indicates aspect ratio.

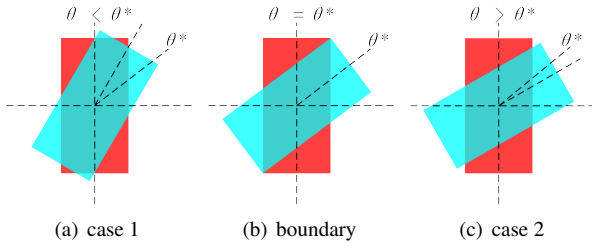


Figure 3. Two situations of SkewIoU calculation.

prior anchor design and NMS. In recent years, DETR has progressed a lot and also exhibits its strong ability in object detection compared with classic detection method [51, 20, 11, 46, 29, 15]. Deformable DETR [51] proposes a deformable attention module to sample the value of adaptive positions around the reference point and utilize the multi-level features to mitigate the slow convergence and high complexity issues of DETR. DAB-DETR [15] provides explicit positional prior for each query to let the cross-attention module focus on a local region corresponding to a target object by using anchor box size. DN-DETR [11] and DINO [46] design a de-noising auxiliary task that bypass the bipartite graph matching, which not only accelerates training convergence but also achieves a better training result. In addition, there have been some DETR-based oriented object detectors [19, 3]. O<sup>2</sup>DETR [19] is the first attempt to apply DETR to the oriented object detection task and AO<sup>2</sup>-DETR [3] introduces oriented proposal generation and refinement module into the transformer architecture to refine the feature. Nevertheless, both of them predict angle in a naive regression way and do not deal with boundary discontinuity and embed angle information into DETR.

### 3. Rethinking High-Precision Detection

At present, the accuracy of oriented object detection is mostly measured by AP<sub>50</sub> [4, 38, 6, 44], which indicates that if the Skew Intersection of Union (SkewIoU) between

the predicted box and ground truth must be greater than 0.5 to be determined as true positive. In order to better observe the relationship between the angle and this metric, we assume that there are two bounding boxes with the same center, width and height. There is a critical angle boundary threshold ( $\theta^* = 2 \arctan \frac{1}{k}$ ) as shown in Fig. 3, then the SkewIoU can be calculated by Eq. 1.

$$\text{SkewIoU}(k, \Delta\theta) = \begin{cases} \frac{4k \tan \frac{\Delta\theta - x - y}{2}}{4k \tan \frac{\Delta\theta + x + y}{2}} & \Delta\theta \leq 2 \arctan \frac{1}{k} \\ \frac{4}{8k \sin \Delta\theta - 4} & \Delta\theta > 2 \arctan \frac{1}{k} \end{cases}$$

$$x = (1 - k \tan \frac{\Delta\theta}{2})^2 \tan^2 \Delta\theta$$

$$y = (\frac{-2 \sin^2 \frac{\Delta\theta}{2} + k \sin \Delta\theta}{\cos \Delta\theta})^2 \quad (1)$$

where  $k \geq 1$  is the aspect ratio, and  $\Delta\theta \in [0^\circ, 90^\circ]$  is the angle deviation.

Fig. 2(a) shows the curve between SkewIoU and angle deviation under different aspect ratios. It can be seen that the SkewIoU variation trend of bounding boxes with different aspect ratio are obviously divided into two types, and dividing boundary is  $ar = 0.5$ , as shown in Fig. 2(b) ( $1 \leq ar \leq 1.5$ ) and Fig. 2(c) ( $ar > 1.5$ ), respectively. Specifically, Fig. 2(b) shows that when the aspect ratio is smaller than 1.5, SkewIoU is always greater than 0.5 regardless of the angle deviation (see *dashed line*). In contrast, when the aspect ratio is greater than 1.5, as shown in Fig. 2(c), SkewIoU will decay rapidly with the increase of angle deviation, but the valid angle deviation still retains a wide range. In summary, objects with a small aspect ratio are insensitive to the angle deviation, whereas objects with a large aspect ratio are sensitive but still have a large tolerance of angle deviation.

Considering that angle is a very important parameter in oriented object detection, the accuracy of its estimation will greatly affect the subsequent related tasks, such as object fine-grained recognition [25], object heading estimation [35, 37], etc., AP<sub>50</sub> seems not suitable for oriented object detection, especially for high-precision detection. There-

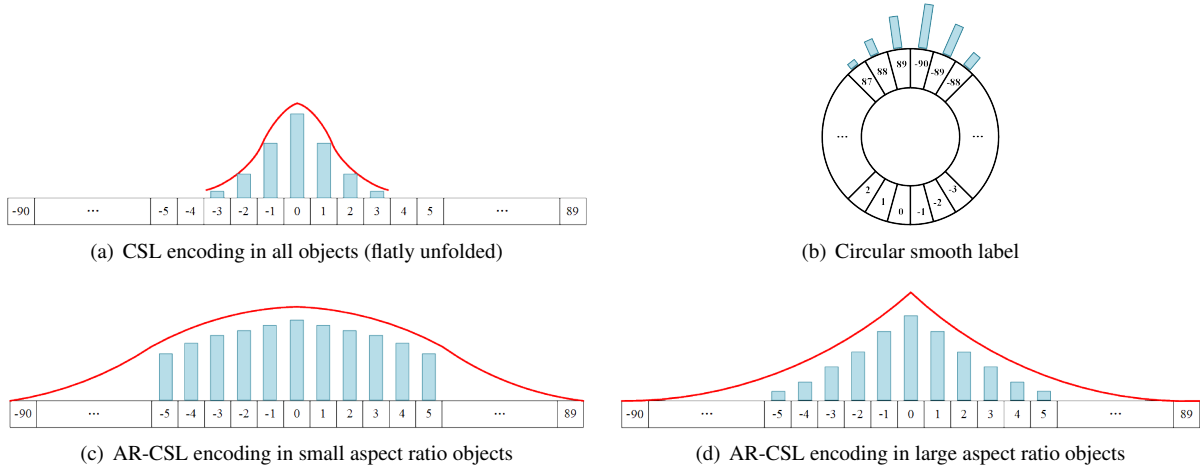


Figure 4. The comparison of two encoding methods in objects with different aspect ratio at each angle deviation. For the convenience of comparison, the labels in the Fig. (a) and Fig. (c)-(d) are flatly unfolded, otherwise they should be circular like (b). (a) For CSL, a Gaussian window with a fixed window radius will be adopted to smooth the angle label, regardless of the objects’ aspect ratio. (c)-(d) For AR-CSL, objects with different aspect ratio will be considered and it will use a more reasonable smoothing strategy to reflect the correlation among the adjacent angles.

fore, we advocate to use more stringent metric, e.g.  $AP_{75}^1$ . As shown the *gray line* in Fig. 2, if  $AP_{75}$  is adopted, regardless of the aspect ratio, the angle deviation is required to be controlled within a certain area otherwise they will not be judged as positive. The larger the aspect ratio, the smaller the area.

Tab. 1 compares the accuracy of some oriented object detectors using  $AP_{50}$  and  $AP_{75}$ , respectively. It can be seen that all detectors achieve a high performance in terms of  $AP_{50}$  and the gap among them is small. However, the situation becomes different when  $AP_{75}$  is used, some detectors may not be good as other detectors whose performance on  $AP_{50}$  are lower than them, e.g.  $S^2A$ -Net vs. Rotated ATSS. Besides, w/ and w/o angle parameter in evaluation, the gap between  $AP_{50}$  and  $AP_{50-H}$  is relatively small while rapidly expanding between  $AP_{75}$  and  $AP_{75-H}$ , which means  $AP_{75}$  pays more attention to the angle prediction.

## 4. Method

### 4.1. Background on Circular Smooth Label

Instead of using regression-based loss function, Circular Smooth Label (CSL) [36] transforms angle prediction into a classification task so that the boundary issue naturally disappears. As shown in Fig. 4(a) and Fig. 4(b), CSL divides the angle into 180 categories and treats the first angle category and the last angle category as adjacent angle categories to eliminate the impact of boundary discontinuity. Then, it adopts Gaussian window function to smooth the

<sup>1</sup>**Note:** The challenge of achieving high  $AP_{75}$  in oriented object detection is more difficult than that in horizontal object detection, because the rotated bounding box is more accurate with less redundant areas, thus more sensitive to errors.

Method	$AP_{50-H}$	$AP_{50}$	$AP_{75-H}$	$AP_{75}$
Rotated ATSS [47]	71.56	72.29	45.10	37.81
Rotated FCOS [26]	72.30	71.88	44.34	37.30
$S^2A$ -Net [6]	72.52	73.91	42.09	35.52
Oriented Reppoints [13]	72.75	71.71	47.62	41.39
Rotated Faster RCNN [23]	75.37	73.40	49.18	39.61
Oriented RCNN [32]	75.49	75.68	53.78	47.17
Gliding Vertex [33]	75.62	73.22	52.37	37.47

Table 1. Accuracy of some oriented object detectors on DOTA-v1.0. ‘1x’ training schedule is used. ‘-H’ indicates to convert the prediction result into a horizontal circumscribing rectangle and evaluate it in DOTA’s horizontal object detection track.

angle category label of the objects so as to reflect the correlation among adjacent angle categories and make it have a certain tolerance for angle estimation error.

Although CSL has made some progress, it still has two drawbacks which will behind its performance:

- **Fixed label function.** CSL adopts a fixed radius Gaussian function to learn the correlation among adjacent angles and smooth the label, without considering objects’ aspect ratio, as shown in Fig. 4(a). However, it can be obviously seen from the Fig. 2 that the SkewIoU of objects with different aspect ratio differs a lot in adjacent angles. Therefore, the correlation among adjacent angles should be not fixed and Gaussian window is probably not the best choice adapted by all objects.
- **Hyperparameter introduction.** The radius of window function will greatly affect the final performance according to Tab. 7. As a hyperparameter, it is a thorny problem to determining the best value of the radius when the dataset used changes.



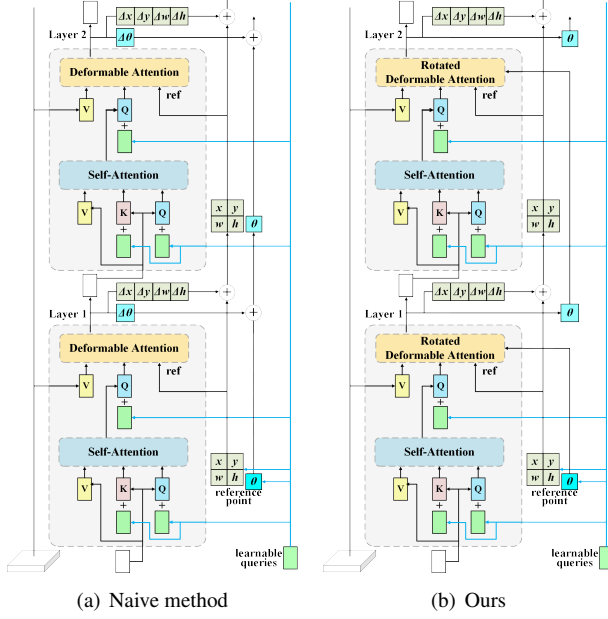


Figure 5. Two methods to iterate the angle information in the DETR. (a) In the naive way, although the angle information is updated iteratively after each layer, it is not embed into DETR. (b) In our proposed way, the angle information will be replaced with a new value after each layer and the angle information will assist in aligning features.

## 4.2. Aspect Ratio Aware Circle Smooth Label

According to the above analysis, the fixed window function and hyperparameter (i.e. radius) hurt the applicability of classification based oriented object detectors to some extent. In this section, we will solve the above issues from the perspective of the encoding form.

Considering that SkewIoU can dynamically reflect the correlation among adjacent angles of different objects, we design an Aspect Ratio aware Circle Smooth Label (AR-CSL) technique to obtain a more reasonable angle prediction, using the SkewIoU instead of a fixed window function to smooth the label. Specifically, we calculate the SkewIoU of the bounding boxes under each angle deviation according to Eq. 1, and take the calculated value as the label of the current angle category bin.

Then, we standardize the SkewIoU values by maximum and minimum normalization method, as shown in follows:

$$\text{AR-CSL}(k, \Delta\theta) = \frac{\text{SkewIoU}(k, \Delta\theta) - \text{SkewIoU}(k)_{\min}}{1 - \text{SkewIoU}(k)_{\min}} \quad (2)$$

where  $k$  is aspect ratio of ground truth.

Compared to CSL, the proposed AR-CSL has the following two advantages:

- **Dynamic label function.** The smoothing values dynamically calculated according to the aspect ratio of

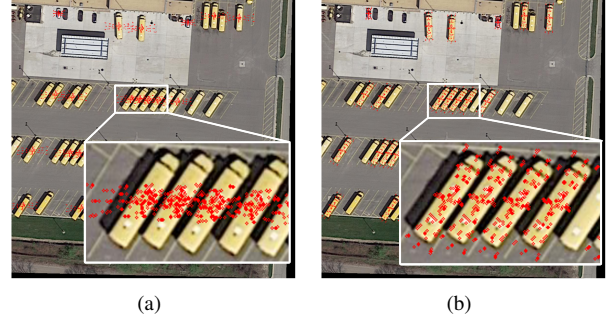


Figure 6. (a) The sampling points is misaligned with objects in Deformable Attention Module. (b) While sampling points is aligned in Rotated Deformable Attention Module.

objects by using SkewIoU, as shown in Fig. 4(c)-4(d).

- **Hyperparameter free.** According to Eq. 1 and Eq. 2, no hyperparameters are introduced, which makes the use of the proposed method more convenient.

## 4.3. Rotated Deformable Attention Module

Fig. 5(a) shows a naive DETR-based oriented detector [19, 3], which only add an additional angle parameter on the heads to achieve rotated bounding box estimation. However, it does not embed the angle information into the detector to exploit the maximum potential of the detector. Specifically, we find that this naive approach will lead to feature misalignment in the whole detector, especially in its deformable attention modules, as shown in Fig. 6(a) and Fig. 7(b).

As depicted in Fig. 7(a), the sampling points in Deformable Attention Module will be adjusted according to the corresponding reference box, so that the sampling points will be restricted within the reference box and fall within the objects as far as possible. However, as shown in Fig. 7(b), when the object are the oriented type, the sampling points cannot accurately align the objects if the horizontal reference box [3] are still used. Therefor, we design a Rotated Deformable Attention Module to align the sampling points with feature by rotating the sampling points according to the embedded angle information, as shown in Fig. 7(c) and Fig. 7(d). The visualization of aligned sampling points are also shown in Fig. 6(b). Moreover, instead of refining the angle layer by layer, we predict a new angle after each layer independently, as shown in Fig. 5(b).

## 4.4. Denoising Training

In order to further improve the performance of the DETR-based model, we adopt the DeNoising (DN) training strategy from DINO [46]. However, there is a bit of difference in adding the noise  $\theta'$  to objects' angle. Instead of method adopted by the class, which randomly flips the class labels to other labels, we define  $\lambda$  as the noise scale

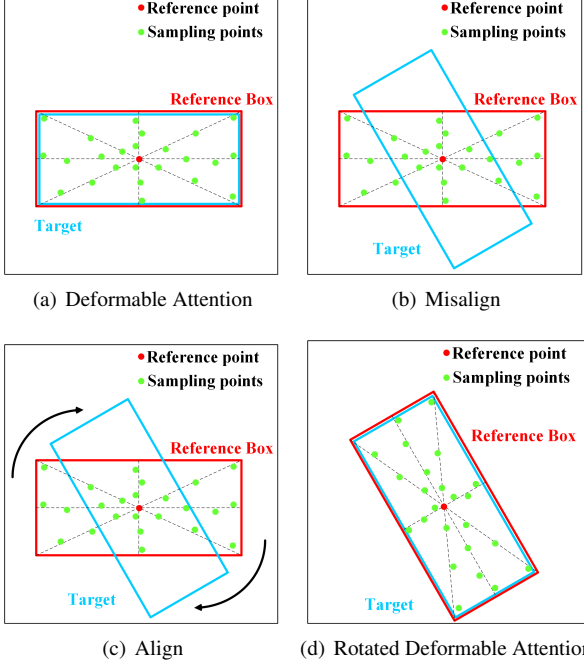


Figure 7. Illustration the misalignment in Deformable Attention and the alignment in Rotated Deformable Attention.

of angle noise  $\Delta\theta$  to make sure that  $|\Delta\theta| < \lambda\bar{\theta}$ , where  $\bar{\theta}$  is the total angle categories and its default value is 180. The expression of adding angle noise is as follows:

$$\theta' = g(\theta + \Delta\theta) \quad (3)$$

where  $g(\cdot)$  is a periodic function to guarantee the value of  $\theta + \Delta\theta$  is within the definition range.

#### 4.5. Aspect Ratio Sensitive Weighting and Matching

Considering the objects with larger aspect ratio are more sensitive to the angle deviation, we also modify the angle loss function and matching cost in the DETR. The expressions are as follow:

$$L_\theta \rightarrow \frac{k}{k+1} L_\theta, \quad C_\theta \rightarrow \frac{k}{k+1} C_\theta \quad (4)$$

where  $k$  is the aspect ratio of the objects.

After modification, the objects with large aspect ratio will be matched to those bounding boxes whose angle is more similar with theirs and the requirement for angle accuracy will also increase in the angle loss calculation. Thus, the model can flexibly adjust the training strategy for different aspect ratio objects.

## 5. Experiments

### 5.1. Datasets and Implementation Details

DOTA-v1.0 [30] is one of the largest datasets for oriented object detection, containing 2,806 large aerial images

from different sensors and platforms ranging from around  $800 \times 800$  to  $4,000 \times 4,000$  and 188,282 instances. We use both training and validation sets for training, and the test set for testing. We divide the images into  $1024 \times 1024$  sub-images with an overlap of 200 pixels. During the training, only the random horizontal, vertical, diagonal flipping is adopted to avoid over-fitting and no other tricks are utilized. The performance of the test set is evaluated on the official DOTA evaluation server.

DIOR-R [2] is an aerial image dataset annotated by oriented bounding boxes from the DIOR [12] dataset. There are 23,463 images and 192,518 instances in this dataset, containing 20 common categories.

OHD-SJTU [37] is a public dataset for oriented object detection and object heading detection. It contains two different scale datasets, called OHD-STJU-S and OHD-SJTU-L. OHD-SJTU-S collects 43 large scene images ranging from  $10,000 \times 10,000$  to  $16,000 \times 16,000$  and 4,125 instances in this dataset. In contrast, OHD-SJTU-L adds more categories and instances, containing six object categories and 113,435 instances. In line with previous work [39, 37] processing, we divide the images into  $600 \times 600$  sub-images with an overlap of 150 pixels and scale it to  $800 \times 800$ .

All models in this paper are implemented by PyTorch [22] based framework MMRotate [50], and trained with AdamW [17] optimizer. The initial learning rate is  $10^{-4}$  with 2 images per mini-batch with default ‘3x’ training schedule. In addition, we adopt learning rate warm-up for 500 iterations, and the learning rate is divided by 10 at decay step.

### 5.2. Main Results

**Results on DOTA-v1.0.** We report the results of 16 oriented object detectors in Tab. 2. Since different methods use different image resolution with different data pre-processing, data augmentation, backbone, training strategies, various tricks and etc. in the original papers, we implement all detectors on MMRotate [50], using the same setting to make the comparison as fair as possible. All the results were obtained by single-scale training and testing, and adopted the ‘3x’ (36 epochs) training schedule. Compared with other angle classification methods (e.g. CSL [36], PSC [45]) or DETR-based detectors (e.g. AO<sup>2</sup>-DETR [3]), AR-CSL has significant advantages in high-precision indicators. With R-50 and Swin-T as the backbone, our method obtain 73.78% and 75.79% on AP<sub>50</sub>, and 49.01% and 51.11% on AP<sub>75</sub>, respectively, which has surpassed other advanced oriented object detection methods on AP<sub>75</sub>.

**Results on DIOR-R.** We also test several advanced oriented detectors on the DIOR-R and summarize the results in Tab. 3. All methods adopt ‘3x’ training schedule and use R-50 as backbone. ARS-DETR achieves the best performance, about 65.90% and 45.11% on AP<sub>50</sub> and AP<sub>75</sub>,

Method	Backbone	PL	BD	BR	GTF	SV	LV	SH	TC	BC	ST	SBF	RA	HA	SP	HC	AP <sub>50</sub>	AP <sub>75</sub>
AO <sup>2</sup> -DETR [3]	R-50	87.99	79.46	45.74	66.64	78.90	73.90	73.30	90.40	80.55	85.89	55.19	63.62	51.83	70.15	60.04	70.91	22.60
Rotated D-DETR [51]	R-50	78.95	68.64	32.57	55.17	72.53	57.77	73.71	88.36	75.46	79.34	45.36	53.78	52.94	66.35	50.38	63.42	26.92
H2RBox [43]	R-50	88.24	79.30	42.76	55.79	78.90	72.70	77.54	90.85	81.96	84.38	55.28	64.49	61.91	70.63	51.51	70.41	37.24
Gliding Vertex [33]	R-50	81.38	77.65	49.33	68.93	73.68	75.97	86.20	90.88	80.55	78.47	57.05	62.56	67.86	71.13	57.33	71.93	39.06
Rotated FCOS [26]	R-50	88.52	77.54	47.06	63.78	80.42	80.50	87.34	90.39	77.83	84.13	55.45	65.84	66.015	72.77	49.17	72.45	39.84
S <sup>2</sup> A-Net [6]	R-50	89.26	84.11	51.97	72.78	78.23	79.41	87.46	90.85	85.62	84.09	60.18	65.90	72.54	71.59	55.31	75.29	40.08
Rotated RetinaNet [14]	R-50	87.33	78.91	46.45	69.81	67.72	62.34	73.59	90.85	82.79	79.37	59.62	61.89	65.01	67.76	44.95	69.23	40.96
PSC [45]	R-50	88.27	73.20	44.55	62.29	77.79	77.30	87.04	90.88	78.47	72.01	52.69	61.14	66.36	69.68	58.10	70.65	40.78
R <sup>3</sup> Det [39]	R-50	89.24	83.32	48.03	72.52	77.52	76.72	86.48	90.89	82.33	83.51	60.96	63.09	67.58	69.27	49.50	73.40	41.69
KLD [42]	R-50	89.13	79.94	51.23	72.56	78.24	78.90	87.10	90.87	85.01	83.81	59.84	64.83	69.92	70.48	55.35	74.48	42.15
KFIoU [44]	R-50	89.20	76.40	51.64	70.15	78.31	76.43	87.10	90.88	81.68	82.22	64.65	64.84	66.77	70.68	49.52	73.37	42.71
GWD [40]	R-50	89.34	80.07	41.94	72.58	79.76	69.93	85.38	90.76	83.16	82.38	62.75	66.06	60.82	69.39	57.84	72.81	42.81
Rotated Faster RCNN [23]	R-50	89.09	78.28	48.93	71.54	74.01	74.99	85.90	90.84	86.87	85.03	57.97	69.74	68.10	71.28	56.88	73.96	43.44
Rotated D-DETR w/ CSL [36]	R-50	86.27	76.66	46.64	65.29	76.80	76.32	87.74	90.77	79.38	82.36	54.00	61.47	66.05	70.46	61.97	72.15	44.07
SASM [9]	R-50	87.51	80.15	51.07	70.35	74.95	75.80	84.23	90.90	80.87	84.93	58.51	65.59	69.74	70.18	42.31	72.47	44.21
Rotated ATSS [47]	R-50	88.94	79.89	48.71	70.74	75.80	74.02	84.14	90.89	83.19	84.05	60.48	65.06	66.74	70.14	57.78	73.37	44.95
CFA [5]	R-50	88.34	83.09	51.92	72.23	79.95	78.68	87.25	90.90	85.38	85.71	59.63	63.05	73.33	70.36	47.86	74.51	46.55
Oriented RCNN [32]	R-50	89.23	77.97	54.05	73.38	74.44	78.07	87.93	90.54	77.08	84.68	61.38	65.54	76.27	70.96	51.39	74.19	46.96
ReDet [7]	R-50	88.94	78.07	51.19	72.76	74.26	78.08	87.44	90.84	80.79	78.59	60.85	64.22	76.84	72.79	54.85	74.03	48.44
ReDet [7]	ReR-50	89.35	76.79	53.12	70.94	73.52	77.41	87.94	90.89	86.98	86.25	67.93	61.62	76.81	69.59	59.84	75.27	49.57
RoI Trans. [4]	R-50	89.01	77.48	51.64	72.07	74.43	77.55	87.76	90.81	79.71	85.27	58.36	64.11	76.50	71.99	54.06	74.05	46.54
RoI Trans. [4]	Swin-T	88.44	85.53	54.56	74.55	73.43	78.39	87.64	90.88	87.23	87.11	64.25	63.27	77.93	74.10	60.03	<b>76.49</b>	<b>50.15</b>
ARS-DETR	R-50	86.61	77.26	48.84	66.76	78.38	78.96	87.40	90.61	82.76	82.19	54.02	62.61	72.64	72.80	64.96	73.79	49.01
ARS-DETR	Swin-T	87.78	78.58	52.58	67.69	80.19	84.32	88.19	90.68	85.92	84.76	55.18	66.89	74.57	79.09	60.35	<b>75.79</b>	<b>51.11</b>

Table 2. Comparisons with the advanced oriented detectors on DOTA-v1.0. R-50 indicates ResNet50 [8]. Swin-T indicates Swin-Transformer [16]. ReR-50 indicates ReResNet50 [6]. **Red** and **blue**: top two performances. D-DETR means Deformable DETR [51].

Method	APL	APO	BF	BC	BR	CH	ESA	ETS	DAM	GF	GTF	HA	OP	SH	STA	STO	TC	TS	VE	WM	AP <sub>50</sub>	AP <sub>75</sub>
Rotated RetinaNet [14]	59.54	25.03	70.08	81.01	28.26	72.02	55.35	56.77	21.26	65.70	70.28	30.52	44.37	77.02	59.01	59.39	81.18	38.43	39.10	61.58	54.83	33.94
SASM [9]	61.41	46.03	73.22	82.04	29.41	71.03	69.22	53.91	30.63	70.04	77.02	39.33	47.51	78.62	66.14	62.92	79.93	54.41	40.62	63.01	59.81	38.22
S <sup>2</sup> A-Net [6]	67.98	44.44	71.63	81.39	42.66	72.72	79.03	70.40	27.08	75.56	81.02	43.41	56.45	81.12	68.00	70.03	87.07	53.88	51.12	65.31	64.50	38.24
R <sup>3</sup> Det [39]	62.55	43.44	71.72	81.48	36.49	72.63	79.50	64.41	27.02	77.36	77.17	40.53	53.33	79.66	69.22	61.10	81.54	52.18	43.57	64.13	61.91	38.40
Gliding Vertex [33]	62.67	38.56	71.94	81.20	37.73	72.48	78.62	69.04	22.81	77.89	82.13	46.22	54.76	81.03	74.88	62.54	81.41	54.25	43.22	65.13	62.91	40.00
GWD [40]	69.68	28.83	74.32	81.49	29.62	72.67	76.45	63.14	27.13	77.19	78.94	39.11	42.18	79.10	70.41	58.69	81.52	47.78	44.47	62.63	60.31	40.90
KLD [42]	66.52	46.80	71.76	81.43	40.81	78.25	79.23	66.63	29.01	78.68	80.19	44.88	57.23	80.91	74.17	68.02	81.48	54.63	47.80	64.41	64.63	41.60
Rotated Faster RCNN [23]	63.07	40.22	71.89	81.36	39.67	72.51	79.19	69.45	26.00	77.93	82.28	46.91	53.90	81.03	75.77	62.54	81.42	54.50	43.17	65.73	63.41	41.80
Rotated FCOS [26]	62.31	42.18	75.34	81.32	39.26	74.89	77.42	68.67	26.00	73.94	78.73	41.28	54.19	80.61	66.92	69.17	87.20	52.31	47.08	65.21	63.21	42.02
Rotated ATSS [47]	62.19	44.63	71.55	81.42	41.08	72.37	78.54	67.50	30.56	75.69	79.11	42.77	56.31	80.92	67.78	69.24	81.62	55.45	47.79	64.10	63.52	42.61
RoI Trans. [4]	63.18	44.33	71.91	81.26	42.19	72.64	79.30	69.67	29.42	77.33	82.88	48.09	57.03	81.18	77.32	62.45	81.38	54.34	43.91	66.30	64.31	43.24
CFA [5]	61.10	44.93	77.62	84.67	37.69	75.71	82.68	72.03	33.41	77.25	79.94	46.20	54.27	87.01	70.43	69.58	81.55	55.51	49.53	64.92	<b>65.25</b>	43.41
ReDet [7]	63.22	44.18	72.11	81.26	43.83	72.72	79.10	69.78	28.45	78.69	77.18	48.24	56.81	81.17	69.17	62.73	81.42	54.90	44.04	66.37	63.81	44.02
Oriented RCNN [32]	63.31	43.10	71.89	81.17	44.78	72.64	80.12	69.67	33.78	77.92	83.11	46.29	58.31	81.17	74.54	62.32	81.29	56.30	43.78	65.26	64.53	<b>44.10</b>
ARS-DETR	65.82	53.40	74.22	81.11	42.13	76.23	82.24	71.52	38.90	75.91	77.91	33.03	57.02	84.82	69.71	72.20	80.33	58.91	51.52	70.73	<b>65.90</b>	<b>45.11</b>

Table 3. Comparisons with the advanced oriented detectors on DIOR-R. All methods adopt ‘3x’ training schedule and use R-50 as backbone. **Red** and **blue**: top two performances.

Method	PL	SH	AP <sub>50</sub>	AP <sub>75</sub>	AP <sub>50:95</sub>
RRPN [18]	90.14	76.13	83.13	27.87	40.74
R <sup>2</sup> CNN [10]	90.91	77.66	84.28	55.00	52.80
RetinaNet-H [39]	90.86	66.32	78.59	58.45	53.07
R <sup>3</sup> Det [39]	90.82	85.59	88.21	67.13	56.19
RetinaNet-R [39]	90.82	85.59	89.48	74.62	61.86
OHDet [37]	90.74	87.59	<b>89.06</b>	<b>78.55</b>	<b>63.94</b>
ARS-DETR	90.61	89.03	<b>89.81</b>	<b>79.94</b>	<b>64.87</b>

Table 4. Comparisons with the advanced oriented detectors on OHD-SJTU-S. **Red** and **blue**: top two performances.

respectively.

**Results on OHD-SJTU.** We compare the performance of some oriented object detection methods on OHD-SJTU, mainly include R2CNN, RRPN, RetinaNet, R<sup>3</sup>Det, OHDet. Without any bells and whistles, our ARS-DETR achieves 79.94% and 45.01% on AP<sub>75</sub> in OHD-SJTU-S and OHD-SJTU-L respectively, surpassing other advanced oriented object detectors. The detail results are shown in Tab. 4 and Tab. 5.

It can be seen from the comparison that although some

Method	PL	SH	SV	LV	HA	HC	AP <sub>50</sub>	AP <sub>75</sub>	AP <sub>50:95</sub>
RRPN [18]	89.55	82.60	57.36	72.26	63.01	45.27	68.34	22.03	31.12
R <sup>2</sup> CNN [10]	90.02	80.83	63.07	64.16	66.36	55.94	70.06	32.70	35.44
RetinaNet-H [39]	90.22	80.04	63.32	63.49	63.73	53.77	69.10	35.90	36.89
R <sup>3</sup> Det [39]	89.89	87.69	65.20	78.95	57.06	53.50	72.05	36.51	38.57
RetinaNet-R [39]	90.00	86.90	63.24	86.90	62.85	52.35	<b>72.78</b>	40.13	40.58
OHDet [38]	89.73	86.63	61.37	78.80	63.76	54.62	<b>72.49</b>	<b>43.60</b>	<b>41.29</b>
ARS-DETR	88.63	87.32	63.60	77.34	69.32	44.01	71.71	<b>45.01</b>	<b>42.56</b>

Table 5. Comparisons with the advanced oriented detectors on OHD-SJTU-L. **Red** and **blue**: top two performances.

methods achieve a good performance on AP<sub>50</sub>, their performance drop significantly when the metric becomes stringent and even worse than other methods whose results on AP<sub>50</sub> are lower than them. In short, this paper mainly advocates the use of more representative indicators (e.g. AP<sub>75</sub>) to study high-precision oriented object detector.

### 5.3. Ablation Studies

**Ablation study of different angle prediction ways in DETR.** The prediction types of angle mainly include regression and classification, and each type can be divided into ways: direct prediction ( $\theta = \theta_{pred}$ ) or indirect pre-

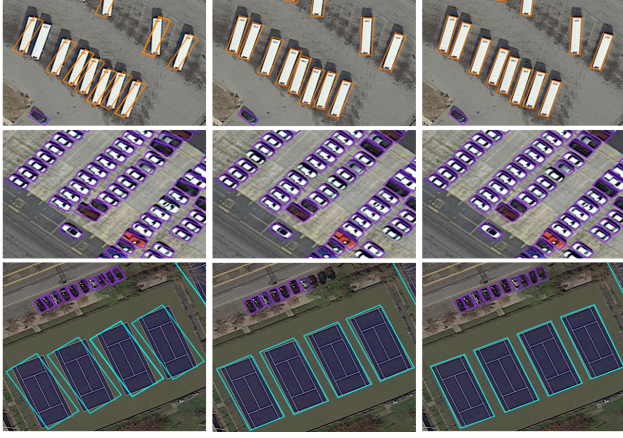


Figure 8. Visual comparison among the Reg. (left), CSL (middle) and AR-CSL (right) on DOTA-v1.0.

diction ( $\theta = \theta_{ref} + \Delta\theta_{pred}$ ). Tab. 6 compares the four combinations and finds that the prediction based on classification is generally better than regression, especially on  $AP_{75}$ . In addition, the way of direct prediction is the best in both types.

#### Ablation study of different angle prediction methods.

Tab. 7 compares the different angle prediction methods on DOTA-v1.0 dataset. As the conclusion in CSL [38], classification is better than regression in angle prediction, 72.15% vs. 63.42%. However, the performance of CSL is vulnerable to the influence of the hyperparameter radius ( $R$ ), which needs to be carefully tuned according to different datasets. In contrast, AR-CSL, which is also based on classification prediction, achieves the best performance (about 72.38% in terms of  $AP_{50}$ ) without tuning any hyperparameters. In particular, AR-CSL has performed surprisingly on the high-precision indicator  $AP_{75}$  thanks to its dynamic label smoothing function, 1.64% higher than CSL, at 45.71%. Fig. 8 further verifies the above conclusion.

**Ablation study of Denoising training.** Tab. 8 also verifies the validity of the modified DeNoising (DN) training strategy. DN improves the performance by 1.12% and 1.24% to 73.50% and 46.95% in terms of  $AP_{50}$  and  $AP_{75}$ , respectively.

**Ablation study of Rotated Deformable Attention Module.** To explore the effectiveness of the Rotated Deformable Attention Module (RDA), we perform ablation studies of detector w/ and w/o RDA in Tab. 8. By aligning query and feature, RDA gets 1.37% and 0.7% gains from 46.95% and 48.31% to 48.21% and 49.01%, respectively.

**Ablation study of Aspect Ratio Sensitive Weighting and Aspect Ratio Matching.** To investigate the contribution of the Aspect Ratio Weighting (ARW) and Aspect Ratio Matching (ARM) in angle, we conduct detail ablation studies on Tab. 8. The results clearly show that both the ARW and ARM can effectively improve the performance,

Angle Pred. Type	Angle Pred. Way	$AP_{50}$	$AP_{75}$
Regression	$\theta = \theta_{ref} + \Delta\theta_{pred}$	63.42	26.92
	$\theta = \theta_{pred}$	69.39	40.79
Classification (AR-CSL)	$\theta = \theta_{ref} + \Delta\theta_{pred}$	70.81	40.64
	$\theta = \theta_{pred}$	<b>72.38</b>	<b>45.71</b>

Table 6. Ablation study of different angle prediction types and ways on DOTA-v1.0. Baseline is Rotated Deformable DETR.

Baseline	Angle Method			$AP_{50-H}$	$AP_{50}$	$AP_{75-H}$	$AP_{75}$
	Reg	CSL	AR-CSL				
Rotated Deformable DETR [51]	✓			63.92	63.42	33.41	26.92
		R=2		74.25	72.57	51.60	43.61
		R=4		74.14	72.24	51.25	42.82
		R=6		74.30	72.15	51.95	44.07
		R=8		74.17	72.10	50.82	43.19
			✓	74.56	72.38	51.72	<b>45.71</b>

Table 7. Ablation study of the different angle prediction methods on DOTA-v1.0. ‘R’ demotes hyperparameter radius. ‘-H’ indicates to convert the prediction result into a horizontal circumscribing rectangle and evaluate it in DOTA’s horizontal detection track.

DN	RDA	ARW	ARM	$AP_{50}$	$AP_{75}$
				72.38	45.71
✓				73.50 (+1.12)	46.95 (+1.24)
✓	✓			73.32 (+0.94)	48.32 (+2.61)
✓		✓		73.59 (+1.21)	47.91 (+2.20)
✓			✓	72.94 (+0.56)	47.59 (+1.88)
✓		✓	✓	73.70 (+1.32)	48.31 (+2.60)
✓	✓	✓	✓	<b>73.79 (+1.41)</b>	<b>49.01 (+3.30)</b>

Table 8. Ablation study of ARS-DETR components on DOTA-v1.0. Baseline is Rotated Deformable DETR with AR-CSL.

about 0.96% and 0.64% respectively.

## 6. Conclusion

In this paper, we have detail analyzed the influence of angle deviation in the oriented object detection and identified the flaws of the current metric (i.e.  $AP_{50}$ ) in high-precision oriented object detection. The widely used metric  $AP_{50}$  has a large tolerance in the angle deviation, which cannot very accurately reflect the performance of the oriented object detectors. Therefore, considering the more stringent metric  $AP_{75}$  to measure the performance is more reasonable. Then, we design a high-precision oriented detector named ARS-DETR, which several novel techniques, including a dynamical angle classification label (AR-CSL), rotated deformable attention module (RDA), denoising strategy (DN) and aspect ratio sensitive weighting (ARW) and matching (ARM). Compared with other advanced oriented detectors, ARS-DETR achieves higher detection accuracy especially in the more stringent metric among the various datasets. Furthermore, we hope that this method will promote future works in high-precision oriented object detection.



## References

- [1] Nicolas Carion, Francisco Massa, Gabriel Synnaeve, Nicolas Usunier, Alexander Kirillov, and Sergey Zagoruyko. End-to-end object detection with transformers. In *European conference on computer vision*, pages 213–229. Springer, 2020. 2
- [2] Gong Cheng, Jiabao Wang, Ke Li, Xingxing Xie, Chunbo Lang, Yanqing Yao, and Junwei Han. Anchor-free oriented proposal generator for object detection. *IEEE Transactions on Geoscience and Remote Sensing*, 60:1–11, 2022. 6
- [3] Linhui Dai, Hong Liu, Hao Tang, Zhiwei Wu, and Pinhao Song. Ao2-detr: Arbitrary-oriented object detection transformer. *IEEE Transactions on Circuits and Systems for Video Technology*, 2022. 2, 3, 5, 6, 7
- [4] Jian Ding, Nan Xue, Yang Long, Gui-Song Xia, and Qikai Lu. Learning roi transformer for oriented object detection in aerial images. In *Proceedings of the IEEE/CVF Conference on Computer Vision and Pattern Recognition*, pages 2849–2858, 2019. 1, 2, 3, 7
- [5] Zonghao Guo, Chang Liu, Xiaosong Zhang, Jianbin Jiao, Xiangyang Ji, and Qixiang Ye. Beyond bounding-box: Convex-hull feature adaptation for oriented and densely packed object detection. In *Proceedings of the IEEE/CVF Conference on Computer Vision and Pattern Recognition*, pages 8792–8801, 2021. 7
- [6] Jiaming Han, Jian Ding, Jie Li, and Gui-Song Xia. Align deep features for oriented object detection. *IEEE Transactions on Geoscience and Remote Sensing*, 60:1–11, 2021. 1, 3, 4, 7
- [7] Jiaming Han, Jian Ding, Nan Xue, and Gui-Song Xia. Redet: A rotation-equivariant detector for aerial object detection. In *Proceedings of the IEEE/CVF Conference on Computer Vision and Pattern Recognition*, pages 2786–2795, 2021. 7
- [8] Kaiming He, Georgia Gkioxari, Piotr Dollár, and Ross Girshick. Mask r-cnn. In *Proceedings of the IEEE/CVF International Conference on Computer Vision*, pages 2961–2969, 2017. 7
- [9] Liping Hou, Ke Lu, Jian Xue, and Yuqiu Li. Shape-adaptive selection and measurement for oriented object detection. In *Proceedings of the AAAI Conference on Artificial Intelligence*, 2022. 7
- [10] Yingying Jiang, Xiangyu Zhu, Xiaobing Wang, Shuli Yang, Wei Li, Hua Wang, Pei Fu, and Zhenbo Luo. R2cnn: rotational region cnn for orientation robust scene text detection. *arXiv preprint arXiv:1706.09579*, 2017. 7
- [11] Feng Li, Hao Zhang, Shilong Liu, Jian Guo, Lionel M Ni, and Lei Zhang. Dn-detr: Accelerate detr training by introducing query denoising. In *Proceedings of the IEEE/CVF Conference on Computer Vision and Pattern Recognition*, pages 13619–13627, 2022. 2, 3
- [12] Ke Li, Gang Wan, Gong Cheng, Liqiu Meng, and Junwei Han. Object detection in optical remote sensing images: A survey and a new benchmark. *ISPRS Journal of Photogrammetry and Remote Sensing*, 159:296–307, 2020. 6
- [13] Wentong Li, Yijie Chen, Kaixuan Hu, and Jianke Zhu. Oriented reppoints for aerial object detection. In *Proceedings of the IEEE/CVF Conference on Computer Vision and Pattern Recognition*, pages 1829–1838, 2022. 4
- [14] Tsung-Yi Lin, Priya Goyal, Ross Girshick, Kaiming He, and Piotr Dollár. Focal loss for dense object detection. In *Proceedings of the IEEE/CVF International Conference on Computer Vision*, pages 2980–2988, 2017. 7
- [15] Shilong Liu, Feng Li, Hao Zhang, Xiao Yang, Xianbiao Qi, Hang Su, Jun Zhu, and Lei Zhang. Dab-detr: Dynamic anchor boxes are better queries for detr. *arXiv preprint arXiv:2201.12329*, 2022. 2, 3
- [16] Ze Liu, Yutong Lin, Yue Cao, Han Hu, Yixuan Wei, Zheng Zhang, Stephen Lin, and Baining Guo. Swin transformer: Hierarchical vision transformer using shifted windows. In *Proceedings of the IEEE/CVF International Conference on Computer Vision*, pages 10012–10022, 2021. 7
- [17] Ilya Loshchilov and Frank Hutter. Decoupled weight decay regularization. In *International Conference on Learning Representations*, 2018. 6
- [18] Jianqi Ma, Weiyan Shao, Hao Ye, Li Wang, Hong Wang, Yingbin Zheng, and Xiangyang Xue. Arbitrary-oriented scene text detection via rotation proposals. *IEEE Transactions on Multimedia*, 20(11):3111–3122, 2018. 2, 7
- [19] Teli Ma, Mingyuan Mao, Honghui Zheng, Peng Gao, Xiaodi Wang, Shumin Han, Errui Ding, Baochang Zhang, and David Doermann. Oriented object detection with transformer. *arXiv preprint arXiv:2106.03146*, 2021. 2, 3, 5
- [20] Depu Meng, Xiaokang Chen, Zejia Fan, Gang Zeng, Houqiang Li, Yuhui Yuan, Lei Sun, and Jingdong Wang. Conditional detr for fast training convergence. In *Proceedings of the IEEE/CVF International Conference on Computer Vision*, pages 3651–3660, 2021. 2, 3
- [21] Qi Ming, Lingjuan Miao, Zhiqiang Zhou, Junjie Song, Yunpeng Dong, and Xue Yang. Task interleaving and orientation estimation for high-precision oriented object detection in aerial images. *ISPRS Journal of Photogrammetry and Remote Sensing*, 196:241–255, 2023. 2
- [22] Adam Paszke, Sam Gross, Francisco Massa, Adam Lerer, James Bradbury, Gregory Chanan, Trevor Killeen, Zeming Lin, Natalia Gimelshein, Luca Antiga, et al. Pytorch: An imperative style, high-performance deep learning library. In *Advances in neural information processing systems*, 2019. 6
- [23] Shaoqing Ren, Kaiming He, Ross Girshick, and Jian Sun. Faster r-cnn: Towards real-time object detection with region proposal networks. In *Advances in Neural Information Processing Systems*, pages 91–99, 2015. 2, 4, 7
- [24] Xuepeng Shi, Shiguang Shan, Meina Kan, Shuzhe Wu, and Xilin Chen. Real-time rotation-invariant face detection with progressive calibration networks. In *Proceedings of the IEEE/CVF Conference on Computer Vision and Pattern Recognition*, pages 2295–2303, 2018. 1
- [25] Xian Sun, Peijin Wang, Zhiyuan Yan, Feng Xu, Ruiping Wang, Wenhui Diao, Jin Chen, Jihao Li, Yingchao Feng, Tao Xu, et al. Fair1m: A benchmark dataset for fine-grained object recognition in high-resolution remote sensing imagery. *ISPRS Journal of Photogrammetry and Remote Sensing*, 184:116–130, 2022. 3
- [26] Zhi Tian, Chunhua Shen, Hao Chen, and Tong He. Fcos: Fully convolutional one-stage object detection. In *Proceedings of the IEEE/CVF International Conference on Computer Vision*, pages 9627–9636, 2019. 4, 7

- [27] Hao Wang, Zhanchao Huang, Zhengchao Chen, Ying Song, and Wei Li. Multigrained angle representation for remote-sensing object detection. *IEEE Transactions on Geoscience and Remote Sensing*, 60:1–13, 2022. 2
- [28] Jian Wang, Fan Li, and Haixia Bi. Gaussian focal loss: Learning distribution polarized angle prediction for rotated object detection in aerial images. *IEEE Transactions on Geoscience and Remote Sensing*, 60:1–13, 2022. 1, 2
- [29] Yingming Wang, Xiangyu Zhang, Tong Yang, and Jian Sun. Anchor detr: Query design for transformer-based detector. In *Proceedings of the AAAI conference on artificial intelligence*, volume 36, pages 2567–2575, 2022. 2, 3
- [30] Gui-Song Xia, Xiang Bai, Jian Ding, Zhen Zhu, Serge Belongie, Jiebo Luo, Mihai Datcu, Marcello Pelillo, and Liangpei Zhang. DOTA: A large-scale dataset for object detection in aerial images. In *Proceedings of the IEEE/CVF Conference on Computer Vision and Pattern Recognition*, pages 3974–3983, 2018. 6
- [31] Zhifeng Xiao, Bin Xu, Yeting Zhang, Kai Wang, Qiao Wan, and Xiaowei Tan. Aspect ratio-based bidirectional label encoding for square-like rotation detection. *IEEE Geoscience and Remote Sensing Letters*, 2023. 2
- [32] Xingxing Xie, Gong Cheng, Jiabao Wang, Xiwen Yao, and Junwei Han. Oriented r-cnn for object detection. In *Proceedings of the IEEE/CVF International Conference on Computer Vision*, pages 3520–3529, 2021. 4, 7
- [33] Yongchao Xu, Mingtao Fu, Qimeng Wang, Yukang Wang, Kai Chen, Gui-Song Xia, and Xiang Bai. Gliding vertex on the horizontal bounding box for multi-oriented object detection. *IEEE Transactions on Pattern Analysis and Machine Intelligence*, 43(4):1452–1459, 2020. 1, 4, 7
- [34] Xue Yang, Liping Hou, Yue Zhou, Wentao Wang, and Junchi Yan. Dense label encoding for boundary discontinuity free rotation detection. In *Proceedings of the IEEE/CVF Conference on Computer Vision and Pattern Recognition*, pages 15819–15829, 2021. 1, 2
- [35] Xue Yang, Hao Sun, Xian Sun, Menglong Yan, Zhi Guo, and Kun Fu. Position detection and direction prediction for arbitrary-oriented ships via multitask rotation region convolutional neural network. *IEEE Access*, 6:50839–50849, 2018. 3
- [36] Xue Yang and Junchi Yan. Arbitrary-oriented object detection with circular smooth label. In *European Conference on Computer Vision*, pages 677–694, 2020. 1, 2, 4, 6, 7
- [37] Xue Yang and Junchi Yan. On the arbitrary-oriented object detection: Classification based approaches revisited. *International Journal of Computer Vision*, 130(5):1340–1365, 2022. 2, 3, 6, 7
- [38] Xue Yang and Junchi Yan. On the arbitrary-oriented object detection: Classification based approaches revisited. *International Journal of Computer Vision*, 130(5):1340–1365, 2022. 3, 7, 8
- [39] Xue Yang, Junchi Yan, Ziming Feng, and Tao He. R3det: Refined single-stage detector with feature refinement for rotating object. In *AAAI Conference on Artificial Intelligence*, volume 35, pages 3163–3171, 2021. 1, 6, 7
- [40] Xue Yang, Junchi Yan, Qi Ming, Wentao Wang, Xiaopeng Zhang, and Qi Tian. Rethinking rotated object detection with gaussian wasserstein distance loss. In *International Conference on Machine Learning*, pages 11830–11841. PMLR, 2021. 1, 7
- [41] Xue Yang, Jirui Yang, Junchi Yan, Yue Zhang, Tengfei Zhang, Zhi Guo, Xian Sun, and Kun Fu. Srdet: Towards more robust detection for small, cluttered and rotated objects. In *Proceedings of the IEEE/CVF International Conference on Computer Vision*, pages 8232–8241, 2019. 1, 2
- [42] Xue Yang, Xiaojiang Yang, Jirui Yang, Qi Ming, Wentao Wang, Qi Tian, and Junchi Yan. Learning high-precision bounding box for rotated object detection via kullback-leibler divergence. *Advances in Neural Information Processing Systems*, 34, 2021. 7
- [43] Xue Yang, Gefan Zhang, Wentong Li, Xuehui Wang, Yue Zhou, and Junchi Yan. H2rbox: Horizontal box annotation is all you need for oriented object detection. In *International Conference on Learning Representations*, 2023. 7
- [44] Xue Yang, Yue Zhou, Gefan Zhang, Jirui Yang, Wentao Wang, Junchi Yan, Xiaopeng Zhang, and Qi Tian. The kfiou loss for rotated object detection. In *International Conference on Learning Representations*, 2023. 3, 7
- [45] Yi Yu and Feipeng Da. Phase-shifting coder: Predicting accurate orientation in oriented object detection. In *Proceedings of IEEE/CVF Conference on Computer Vision and Pattern Recognition*, 2023. 2, 6, 7
- [46] Hao Zhang, Feng Li, Shilong Liu, Lei Zhang, Hang Su, Jun Zhu, Lionel M Ni, and Heung-Yeung Shum. Dino: Detr with improved denoising anchor boxes for end-to-end object detection. In *International Conference on Learning Representations*, 2023. 2, 3, 5
- [47] Shifeng Zhang, Cheng Chi, Yongqiang Yao, Zhen Lei, and Stan Z Li. Bridging the gap between anchor-based and anchor-free detection via adaptive training sample selection. In *Proceedings of the IEEE/CVF conference on computer vision and pattern recognition*, pages 9759–9768, 2020. 4, 7
- [48] Yu Zheng, Danyang Zhang, Sinan Xie, Jiwen Lu, and Jie Zhou. Rotation-robust intersection over union for 3d object detection. In *European Conference on Computer Vision*, pages 464–480, 2020. 1
- [49] Xinyu Zhou, Cong Yao, He Wen, Yuzhi Wang, Shuchang Zhou, Weiran He, and Jiajun Liang. East: an efficient and accurate scene text detector. In *Proceedings of the IEEE/CVF Conference on Computer Vision and Pattern Recognition*, pages 5551–5560, 2017. 1
- [50] Yue Zhou, Xue Yang, Gefan Zhang, Jiabao Wang, Yanyi Liu, Liping Hou, Xue Jiang, Xingzhao Liu, Junchi Yan, Chengqi Lyu, et al. Mmrotate: A rotated object detection benchmark using pytorch. In *Proceedings of the 30th ACM International Conference on Multimedia*, pages 7331–7334, 2022. 6
- [51] Xizhou Zhu, Weijie Su, Lewei Lu, Bin Li, Xiaogang Wang, and Jifeng Dai. Deformable detr: Deformable transformers for end-to-end object detection. In *International Conference on Learning Representations*, 2021. 2, 3, 7, 8